Langmuir

Article

pubs.acs.org/Langmuir

On-Demand Droplet Fusion: A Strategy for Stimulus-Responsive Biosensing in Solution

Praveena Mohan, Patrick S. Noonan, Matthew A. Nakatsuka, and Andrew P. Goodwin*

Department of Chemical and Biological Engineering, University of Colorado Boulder, 3415 Colorado Ave., 596 UCB, Boulder, Colorado 80309, United States

Supporting Information

ABSTRACT: A novel strategy is reported for biochemically controlled fusion of oil-in-water (O/W) droplets as an in-solution sensor for biological targets. Inspired by the SNARE complex in cells, the emulsions were stabilized by a combination of phospholipids, phospholipid−poly(ethylene glycol) conjugates, and cholesterol-anchored oligonucleotides. Prior to oligonucleotide binding, the droplets were stable in aqueous media, but hybridization of the oligonucleotides in a zipperlike fashion was shown to initiate droplet fusion. Using image analysis of content mixing of dye-loaded droplets, fusion specificity was studied and optimized as a function of interfacial chemistry. Changing the orientation of the anchored oligonucleotides, using long-chain phospholipids (C18 and C22), and binding a complementary oligonucleotide slowed or even halted fusion completely. Based on these studies, a sensor for the biomarker thrombin was designed using competitive binding of aptamer strands, with droplet fusion increasing as a function of thrombin addition in accordance with a simple binding model, with sensitivity down to 100 nM and with results in as little as 15 min. Future efforts will focus on utilizing this mechanism of content mixing to facilitate highly sensitive detection via modalities such as magnetoresistance or chemiluminescence.

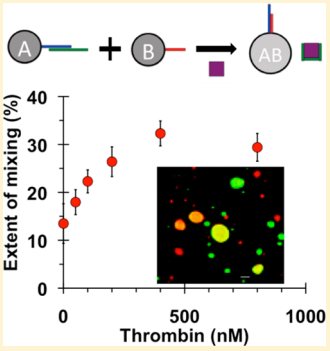

1. INTRODUCTION

The sequestration of molecules and other contents into dispersible colloids is of widespread importance for applications in biotechnology, medicine, and analytics. Confinement of encapsulated contents into droplets allows the dispersal of many different types of molecules in suspension while maintaining their mutual separation. If the droplets do fuse, or coalesce, their contents will be mixed together but still remain separate from other molecules in suspension, allowing selective interaction in a confined volume. While oil droplets dispersed in aqueous media spontaneously fuse to reduce their overall surface area and energy, the use of specific binding events to control droplet fusion is less trivial. Such techniques have been developed for microfluidics,[1−4] in which the flow and channel design help to control the spatial location of each droplet. While microfluidics have been quite successful in analytics, the technique is limited to small volumes and flow rates. A technique that could fuse specific oil-in-water (O/W) droplets together rapidly and in bulk would help to pave the way for in-solution detection of biologics without any washing steps.

In this paper, we present a new methodology for rapid and controlled mixing of specific droplets in bulk suspension. This method was inspired by the *N*-ethyl-maleimide-sensitive-factor attachment protein (SNARE), which induces fusion between cell organelles and membranes. The key step in the SNARE-mediated fusion process is the formation of a four-helix bundle, the formation of which applies a directional force that draws the vesicle and the membrane close to one another and overcomes the entropy loss and steric hindrance associated with lipid mixing.[5,6] This in turn facilitates pore formation between the two membranes, followed by completion of the fusion process. Synthetic mimics of this "zippering process" have been designed in liposome models using simple peptide constructs,[7] peptide-antigen interactions,[8] and oligonucleotides.[9,10] In particular, Höök and coworkers employed DNA−cholesterol conjugates anchored in the outer leaflet as associative groups for initiating liposome fusion.[11−13]

In applying such technologies to O/W emulsions, it was important to demonstrate that the formulations used for liposome bilayers can be adapted to monolayers at the surface of a droplet. Also, the fusion process itself is thermodynamically favored through the consequential reduction in interfacial energy, so additional steric barriers must be added to the monolayer to prevent nonspecific coalescence under normal conditions. In our work with microbubbles and liposomes,[14−17] as well as others' with bubbles, emulsions, and liquid crystal monolayers,[18−23] monolayers consisting of phospholipids and conjugates of poly(ethylene glycol) and 1,2-distearoyl-*sn*-glycero-3-phosphoethanolamine (DSPE-PEG) have proven successful in maintaining stable colloidal suspensions. However, steric barriers are expected to retard specific fusion as well. Thus, careful utilization of both PEG length and DSPE-PEG

Received: June 24, 2014
Revised: September 9, 2014
Published: September 27, 2014

density are necessary for maximizing emulsion fusion specificity.

2. EXPERIMENTAL SECTION

2.1. Materials. 1,2-Dipalmitoyl-*sn*-glycero-3-phosphocholine (DPPC); 1,2- distearoyl-*sn*-glycero-3-phosphocholine (DSPC); 1,2-dibehenoyl-*sn*-glycero-3-phosphocholine (DBPC); and 1,2-distearoyl-*sn*-glycero-3-phosphoethanolamine-*N*-[methoxy(polyethylene glycol)] (ammonium salt) (DSPE-PEG) (PEG molecular weights of 1000, 2000, and 5000) were obtained from Avanti Polar Lipids (Alabaster, AL). 4-Cyano-4′-pentylbiphenyl (5CB) and 9,10-bis(phenylethynyl)-anthracene (BPEA) dye were obtained from TCI America (Portland, OR). Cholesterol-modified DNA sequences (Chol-DNA) and thrombin aptamer (TA) were obtained from Integrated DNA Technologies (Coralville, IA). 1,1′-Dioctadecyl-3,3,3′,3′-tetramethylindocarbocyanine perchlorate (DiI) and 3,3′-dioctadecyloxacarbocyanine perchlorate (DiO) dyes were obtained from Sigma-Aldrich (St. Louis, MO). Chloroform, Tris base, and sodium chloride (NaCl) were obtained from Fisher Scientific (Pittsburgh, PA).

2.2. Preparation of Lipid Stock Solution. Tris buffer of 10 mM Tris base and 100 mM NaCl was prepared, and its pH was adjusted to 8.0 with 1 M HCl. A total of 16 mg of lipid (DPPC, DSPC, or DBPC) was dissolved in 1.5 mL of chloroform and sonicated in a water bath at 32 °C for 2 min until the solution was clear. The solvent was evaporated in a 100 mL round-bottom flask under vacuum in a rotary evaporator for 30 min. Once the chloroform was evaporated and the film was formed, a stock solution of 4 mg/mL lipid was prepared by hydrating the film in 4 mL of Tris buffer. The mixtures were stirred for ca. 40 min in a heated water bath at 75 °C for DPPC and DSPC; and at 90 °C for DBPC.

2.3. Preparation of Chol-DNA Loaded Vesicles and 5CB Emulsions. The lipid/PEG/DNA mixtures were prepared by adding Chol-DNA and DSPE-PEG in aqueous media to the lipid stock solution. The concentration of lipid in the final formulation was 1.3 mM; and Chol-DNA and DSPE-PEG concentrations were adjusted according to the experiments. This mixture was then heated to 75 °C for DPPC and DSPC and at 90 °C for DBPC and stirred for 30 min. Once the solutions were cooled to room temperature, 2 v/v % 5CB was added to the mixtures. The samples were then emulsified using a 40 kHz probe sonicator (Branson SLPe, Branson Ultrasonics, Danbury, CT) with an output power of 120 W. The samples were then centrifuged at 1600*g* for 1 min to remove large and nonencapsulated 5CB droplets. The supernatants were centrifuged again at 6000*g* for 4 min to pellet down the encapsulated 5CB droplets. The supernatant containing excess lipids and smaller droplets (<200 nm) was removed, and the pellet was suspended in Tris buffer

2.4. Fusion Experiments. 5′Chol-DNA and 3′Chol-DNA incorporated vesicles were prepared separately as described above, with either BPEA (green) or DiI (red) predissolved in the 5CB (approx. 200 μg/mL). When the two sets of emulsion were mixed together, DNA-hybridization mediated fusion of droplets was observed by tracking the mixing of red and green dyes. For control groups, green and red emulsions were prepared without Chol-DNA in the initial lipid film. An equal volume of green and red emulsions were mixed together in a microcentrifuge tube and incubated in a shaker at 37 °C. A small amount of sample was removed from this mixture at regular time intervals of 0, 15, 30, 45, and 60 min; and then diluted 25-fold in Tris buffer before imaging. A drop of the sample (8 μL) was placed on a glass slide and immobilized with a coverslip, then imaged with an inverted confocal microscope (Nikon A1R 100X (NA 1.45), Nikon Instruments, Melville, NY). The green and red fluorescence were excited at 488 and 514 nm, respectively, while the emissions were detected through 525/50 and 600/50 band pass emission filters, respectively. The images were obtained over a *Z*-range of −0.8 to +0.8 μm with *Z*-increments of 0.2 μm. Several images (6−10) were taken at each time point. For FRET studies, the droplets with either DiI or DiO dye were excited at 488 nm only while emissions were detected through each band pass filter.

2.5. Image Analysis: Measurement of Fusion and Size Distribution. ImageJ (NIH) was used to select one green and one red channel image from the same focus among the *Z*-stacks and save them separately in a tif format.[24] A MATLAB code (MATLAB and Statistics Toolbox Release 2013a, The MathWorks, Inc., Natick, MA) was written to select droplets found in both channels and then measure the mean intensities and surface area for each droplet. The mixing of red and green dyes was quantified by determining intensity ratio, $I_G/(I_G + I_R)$; thus, a completely red droplet would have a value of 0 and a completely green droplet would have a value of 1. A histogram of intensity ratio versus count was plotted in bin increments of 0.05, and a ratio of summed droplet counts between 0.15 and 0.85 was compared to the total droplet count (see Figure S2, Supporting Information).

2.6. Detection of Thrombin Using Thrombin Aptamer. Emulsions were prepared as above, but during the vesicle preparation step, thrombin aptamer and 5′Chol-DNA were added to the lipid stock and DSPE-PEG solution. This sample was then stirred at 75 °C for 30 min. The formulation contained 1.3 mM DPPC, 40 μM DSPE-PEG2000, 1.0 μM thrombin aptamer, and 0.65 μM Link-1 DNA. The molar ratio of DNA/PEG/lipid was 1:62:2000. Link-2 incorporated vesicles were prepared as before. Again, green and red 5CB emulsions were made with Link-1/TA vesicles and Link-2 vesicles. The fusion experiments were repeated by mixing equal amounts of green and red emulsions with different thrombin concentrations of 0, 50, 100, 200, 400, and 800 nM. The emulsion fusion was imaged at 45 min after mixing, and then processed to report the maximum fusion efficacy over the range of thrombin concentrations.

3. RESULTS AND DISCUSSION

3.1. Preparation of Fusogenic Droplets. To formulate emulsions capable of biochemically directed fusion, two sets of emulsions were prepared with DNA oligonucleotides present at their surface that were complementary to the DNA in the other set of emulsions. In keeping with the SNARE-inspired fusion strategy, the oligonucleotides were designed to hybridize through a "head-to-head" coupling, in which hybridization of DNA on complementary emulsions pulls the lipid monolayers together (Figure 1a), as opposed to a "head-to-tail"

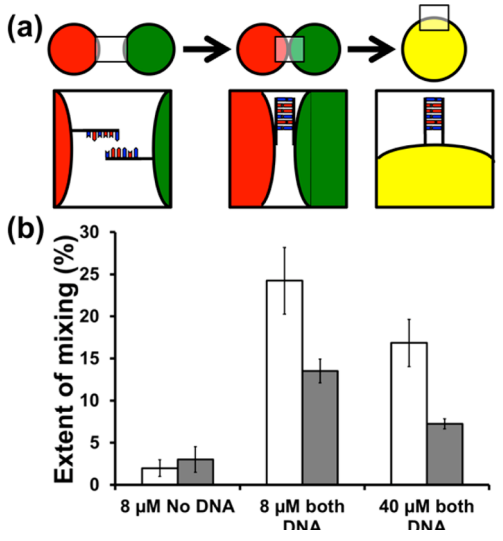

Figure 1. (a) Schematic of emulsion fusion process. Complementary DNA oligonucleotides are placed on emulsions with different contents. DNA hybridization anchors the emulsions together, followed by emulsion fusion. (b) Extent of mixing for DSPE-PEG2000 (white bar) and DSPE-PEG5k (gray bar) stabilized 5CB droplets after 45 min ([DPPC] = 1.3 mM, [Chol-DNA] = 0.85 μM), droplet concentration = 1×10^9 mL^{-1}. Error bars = 95% CI.

dx.doi.org/10.1021/la502483u | *Langmuir* 2014, 30, 12321−12327

conformation that is typical of nanoparticle aggregation schemes.[25−29] In particular, programmable head-to-tail DNA-mediated assembly of O/W droplets into microscopic structures has been demonstrated, and tellingly there was little evidence of content mixing.[30] The DNA was anchored into the membrane through end-functionalization with a cholesteryl group linked to the DNA via a triethylene glycol (TEG) spacer. The two DNA sequences were 5′Chol-TEG/TCC GTC GTG CCT TAT TTC TGA TGT CCA AAA CCA ACC ACA/3′ (hereby Link-1) and 5′/GTT GGT TTT GGA CAT CAG AAA TAA GGC ACG ACG GA/3′Chol-TEG (Link-2). To formulate the emulsions, first 1,2-dipalmitoyl-*sn*-glycero-3-phosphocholine (DPPC) was mixed with DSPE-PEG and the appropriate Chol-DNA sequence. After reconstitution of a film containing these components, 4-cyano-4′-pentylbiphenyl (5CB) was added and the mixture was probe sonicated to form the emulsions, followed by size fractionation via centrifugation. The placement of the DNA within the monolayer was confirmed through additional experiments in which dye-labeled complementary DNA strands hybridized to the emulsion DNA were found to remain after centrifuge washing (Figure S1, Supporting Information).

3.2. Analysis of Droplet Fusion. The fusion of the droplets was followed through the analysis of confocal fluorescence microscopy images. In a typical experiment, two sets of emulsions were prepared, one with Link-1 and containing 9,10-bis(phenylethynyl)anthracene (BPEA, green) dissolved in the 5CB, and the other with Link-2 and 1,1′-dioctadecyl-3,3,3′,3′-tetramethylindocarbocyanine perchlorate (DiI, red) in the 5CB. The samples were mixed and agitated at 37°C, the mixture was diluted, and the sample was imaged in separate green and red fluorescence channels at different time points by confocal microscopy. After adjusting for fluorescence contamination between channels, the fraction of colocalization (i.e., $I_G/(I_G + I_R)$) was determined for each droplet, the results of which were then converted to a histogram such as that shown in Figure S2 in the Supporting Information. Droplets with fractions between 0.15 and 0.85 inclusive were considered fused as determined from thresholds based on experiments using single dyes; those outside that range were considered unfused. Visually, the images appear on a false color range from green (BPEA only) to yellow (equal amounts BPEA and DiI) to red (DiI only).

The extent of droplet fusion was first studied as a function of emulsion monolayer composition. In keeping with published work for liposomes, a DPPC:Chol-TEG-DNA ratio of 1600:1 (1.3 mM DPPC and 0.85 μM Chol-TEG-DNA) was used to prepare emulsions.[12] Importantly, droplets that did not possess DNA failed to undergo significant fusion, with a baseline of ∼3% nonspecific fusion. Next, DSPE-PEG2000 and DSPE-PEG5000 of different molar concentrations (8 and 40 μM) were incorporated into the shell, and the extent of mixing at 45 min was measured (Figure 1b). The highest extent of mixing was obtained for 8 μM DSPE-PEG2000, which adequately reduced nonspecific fusion but increased the efficacy of DNA-driven fusion. The mean diameter of the droplets, as determined from image analysis, prepared with 40 μM PEG2000 was found to be smaller (0.69 ± 0.02 μm) than that of droplets prepared with 8 μM PEG2000 (0.78 ± 0.03 μm) owing to increased droplet stability with higher PEG concentrations. After DNA-driven fusion, the mean diameter of the droplets increased from 0.71 ± 0.01 to 0.78 ± 0.03 μm (Figure S3, Supporting Information), an increase that was consistent with 40% droplet fusion.

One potential criticism of this analytical method may be that the droplets are in fact aggregating, but are small enough that their separation cannot be effectively distinguished by microscopy. To confirm the content-mixing between droplets, fluorescence resonance energy transfer (FRET) studies were conducted using DiI as the acceptor and 3,3′-dioctadecyloxacarbocyanine perchlorate (DiO, green) as the donor. During imaging, the droplets were excited at 488 nm only, but their emissions were recorded in both the green (emission 525/50 nm) and red channels (emission 600/50 nm). The DiO droplets were first imaged in the absence or presence of DiI droplets without complementary DNA (Figure 2a) to obtain a baseline. After DNA-mediated droplet fusion (Figure 2b), the fluorophores would mix to obtain efficient energy transfer, resulting in a decrease in DiO emission and an increase in DiI emission. FRET efficiency was calculated as (1-DiO′/DiO), where DiO and DiO′ are the DiO fluorescence intensities in the absence of and presence of DiI droplets, respectively (Figure 2c). The FRET efficiency was found to be higher for DNA-driven fused droplets, which indicates that content mixing was in fact taking place.

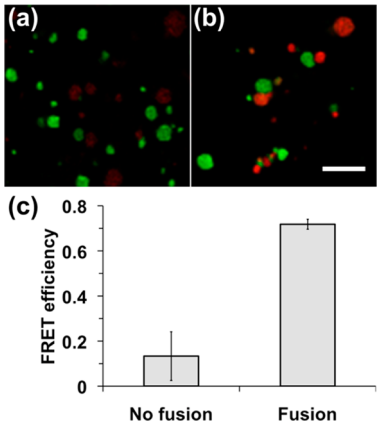

Figure 2. FRET studies: FRET images of 5CB droplets (DiI-red and DiO-green) with no DNA (a) and fused droplets with complementary DNA (b) ([DPPC] = 1.3 mM, [DSPE-PEG2000] = 40 μM, [Chol-DNA] = 0.85 μM and droplet concentration =1.4 × 10^{10} mL^{-1}). Excitation wavelength = 488 nm, and the emission filter used was 525/50 nm. (c) Comparison of FRET efficiency calculated as (1-DiO′/DiO), where DiO′ and DiO is the measured fluorescence intensity of DiO droplets in the presence and absence of DiI droplets, respectively; scale bar is 2 μm; error bars = 95% CI.

3.3. Effect of Interfacial Chemistry on Fusion Efficiency. The chemical properties at the interface of the droplets should have a significant effect on the extent of emulsion fusion. Longer acyl chain phospholipids are known to provide more stability to colloids than their shorter counterparts owing to their higher melting temperature and stronger packing energy.[31] Complementary droplets stabilized with DPPC (C16, T_m = 41 °C) showed an initial aggregation immediately after mixing, with considerable fusion occurring immediately (Figure 3). The droplet concentration was also increased 13-fold (1.4 × 10^{10} mL^{-1}), and the extent of mixing increased to 40−45% (DPPC in Figure 3b) compared to 25% mixing in Figure 1b. While it is expected that more collision events will occur for a higher concentration of droplets, the

dx.doi.org/10.1021/la502483u | *Langmuir* 2014, 30, 12321−12327

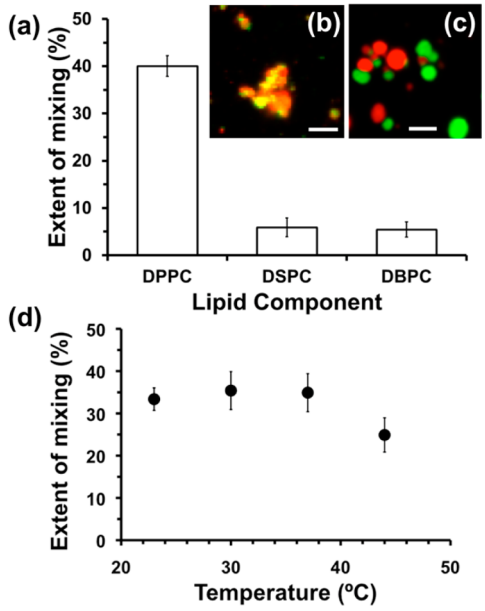

Figure 3. (a) Comparison of percent of mixing between different lipids ([lipid] = 1.3 mM, [Chol-DNA] = 0.85 μM, and [DSPE-PEG2000] = 8 μM), droplet concentration =1.4 × 10^{10} mL^{-1}. (b, c) Fluorescent images of aggregation and/or fusion of DNA-loaded 5CB droplets at 45 min stabilized by (b) DPPC and (c) DSPC. Error bars = 95% CI; scale bar = 2 μm. (d) Extent of mixing (%) plotted against temperatures ranging from 23 to 44 °C ([DPPC] = 1.3 mM, [DSPE-PEG2000] = 40 μM, [Chol-DNA] = 0.85 μM, and droplet concentration =1.4 × 10^{10} mL^{-1}); error bars = 95% CI.

extent of mixing remained less than 5% for droplets without oligonucleotides. Droplets stabilized with DSPC (C18, T_m = 55 °C) and DBPC (C22, T_m = 75 °C) also aggregated, but did not appear to fuse significantly after 60 min (Figure 3a). Thus, the crystalline nature of the longer acyl chains appears to prevent the fusion process entirely.

To test the hypothesis that fusion would occur most readily when the lipids possessed a fluid phase, the effect of temperature on fusion efficiency was studied. In particular, it was important to ascertain if DPPC and 5CB influence DNA-driven droplet fusion, as DPPC transitions from gel to fluid state at 41 °C, and even undergoes a slower pretransition at 28 °C,[32] which is less than the experimental temperature of 37 °C. In addition, 5CB undergoes a phase transition from a crystalline state to a nematic state at 18 °C and then to an isotropic state at 35 °C. Lipid-stabilized 5CB droplets with DiI and BPEA dyes were prepared and incubated for fusion studies as before. The droplets were incubated in a shaker with temperatures ranging from 23 to 44 °C, and the extent of mixing was calculated from the fluorescent images (Figure 3d). There was no significant difference in the extent of mixing over the temperature range of 23−37 °C, but the extent of mixing decreased by approximately 8% at 44 °C. This observation indicates that the DPPC likely plays a greater role in fusion efficiency. We hypothesize that DPPC melting destabilized the lipid shell, releasing the Chol-DNA from the droplets.

3.4. Effect of DNA Orientation on Droplet Fusion. A central hypothesis of this work is that both the presence and orientation of the DNA are vital for obtaining rapid, directed fusion. That is, either orientation of DNA hybridization will cause the emulsions to aggregate initially, but only the head-to-head hybridization of the DNA will facilitate fusion of the droplets by promoting a "zipper" mechanism to bring the two lipid monolayers together. To test this hypothesis, emulsions were formulated from shell compositions of 1.3 mM DPPC, 40 μM DSPE-PEG2000, and 0.85 μM of Chol-TEG-DNA, in which Link-1 and Link-2 represented the head-to-head configuration and the sequence of Link-2 was reversed to obtain a head-to-tail configuration. While droplets with head-to-tail hybridization displayed substantial aggregation immediately after mixing, these droplets fused very little (Figure 4). With

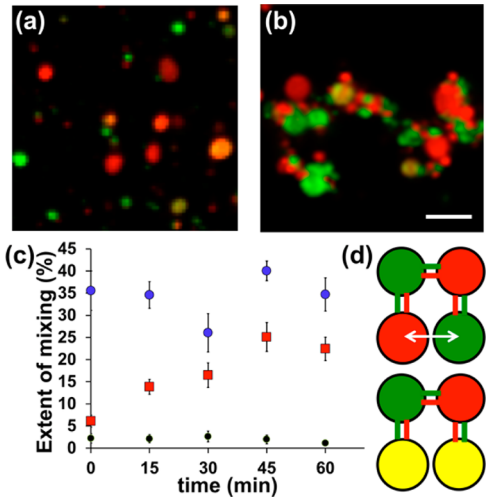

Figure 4. Effect of DNA configuration on extent of mixing. (a, b) Fluorescence images of 5CB droplets ([DPPC] = 1.3 mM, [DSPE-PEG2000] = 8 μM, and [Chol-DNA] = 0.85 μM): (a) head-to-head configuration of Chol-DNA and (b) head-to-tail configuration of Chol-DNA after 15 min. Error bars = 95% CI; scale bar is 2 μm. (c) Extent of mixing of droplets vs time for no DNA (black circles), head-to-head configuration (blue circles), and head-to-tail configuration (red squares). (d) Schematic of possible mechanism of fusion among aggregated droplets containing head−tail configuration DNA.

head-to-head coupling, the droplets aggregated quickly, fused within the first time point taken, and maintained that approximate level of fusion thereafter. Thus, the fusion process proved to be very fast for droplets, with similar results as for liposome fusion.[11−13] Without DNA, the fusion remained at nonspecific background levels, indicating that the DSPE-PEG inhibited nonspecific fusion. Interestingly, after 15 min, the head-to-tail droplets remained in a highly aggregated state, but the number of fused droplets increased to a maximum level of about 25% after 60 min (Figure 4c). In contrast, Boxer and co-workers showed that head-to-tail DNA-mediated vesicle bilayer fusion led only to docking of vesicles on a supported lipid bilayer without fusion or content-mixing,[33] which was supported by droplet studies by Hanczyc and coworkers.[30] Their vesicle composition was 2:1:1 DOPC/DOPE/cholesterol with a 24-base DNA sequence (8 nm), and the lipid mixing experiments showed that there was no fusion. DOPE, with its large polar headgroup without a hydrophobic moiety, can cause destabilization of the outer layer of the vesicle membrane, leading to "hemifusion". As shown by Agirre et al. even when the distance between the vesicles was as large as 14 nm (antibody-mediated vesicle aggregation), the outer layers appeared to fuse while inner contents remained unmixed.[34] With a lipid monolayer, there is no inner leaflet, so fusion may take place, but more slowly than with the head-to-head conformation. A longer 39-base DNA sequence used in our

dx.doi.org/10.1021/la502483u | Langmuir 2014, 30, 12321−12327

reported study would result in about 13 nm of spacing between the tethered droplets (0.33 nm per nucleotide), which should not allow fusion of lipid shell between the tethered droplets. The fusion of some of these droplets may be explained further if the droplets are brought into closer contact through aggregation networks, as exemplified in Figure 4d, along with the gel-state of DPPC monolayer and the curvature of droplets favoring fusion. In our experiments, there appears to be a two-step process in which the emulsions form large aggregates, followed by fusion of a few of the droplets within the clusters. The fusion occurs over a longer incubation time of 30−45 min at 37 °C compared to quicker fusion (<15 min) with head−head DNA configuration. Another difference between the two mechanisms is that after 15 min the head-to-tail droplets remained primarily highly aggregated, but the head-to-head droplets separated into single droplets. We attribute this difference to the potential exchange of one DNA strand from one droplet to the other, as the DNA is held in the monolayer only by one cholesteryl unit. The change in stiffness caused by DNA hybridization places conformational strain on the lipid−cholesterol interaction, which most likely aids the transfer of the DNA−cholesterol conjugate from one monolayer to transfer to the other. Head-to-tail hybridization would not provide this strain, so transfer is likely minimized in this scenario.

3.5. Comparison of Thrombin Detection Using Competitive Aptamer Binding versus Sandwich-Type Binding. One substantial benefit of using DNA strands to mediate fusion is that they can be used to detect biomolecules using aptamers.[35,36] Strategies to employ DNA-aptamer based switches for sensing have included detection using ultrasound,[15,17] fluorescence,[37] electrochemical signal,[38] and other methods.[39−48] To create a system in which emulsion fusion could be regulated by the presence of specific biomolecules, the Link-1 strand was designed to partially hybridize to a DNA aptamer sequence for thrombin 5′/GGT TGG TGT GGT TGG TTT/3′, so that the thrombin aptamer (TA) had affinity for both the target analyte (thrombin) and the oligonucleotide strands on the droplets (Link-1). The dissociation constant (K_d) between the 15-base aptamer and thrombin has been reported to be 200 nM.[49] The Link-1 sequence contains 12 nucleotides on the 3′ end that are complementary to the thrombin aptamer. The K_d for aptamer−Link-1 interactions was predicted using the nearest-neighbor model (free energy at 0.15 M [Na+] and 37 °C) and van't Hoff equation and was found to be 15 nM (calculations in the Supporting Information).[50] When the lipid solution with Link-1 DNA was premixed with excess aptamer, the Link-1 DNA was expected to be bound to the aptamer due to the low dissociation constant. During centrifuge washing of the emulsion, the unbound TA was removed. Assuming a simple competitive binding model and using a Link1 concentration of 135 nM, the amount of Link-1 available for hybridization with Link-2 DNA was estimated at varying thrombin concentrations (Figure 5a). Since the fusion process clearly disrupts the hybridization between Link-1 and Link-2, the model does not take into account this dissociation constant of Link1−Link2 interactions, and therefore, the model is only a semiquantitative estimation of fusion process. The equations used in the assay model and the MatLab code used to solve the equations are detailed in the Supporting Information. From the prediction, an exponential increase in percent of hybridization is expected

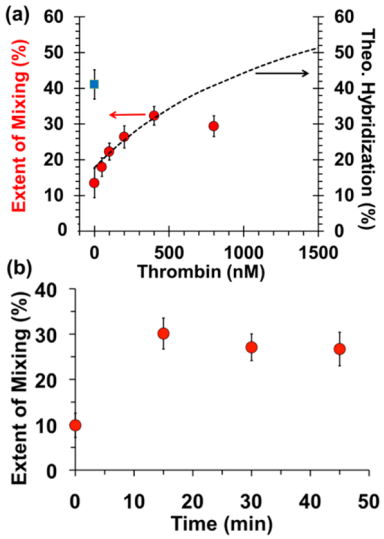

Figure 5. Thrombin dose−response. (a) Extent of mixing (red circles, left *y*-axis) from fusion studies and percent of mixing for droplets without TA (blue square). Extent of mixing of Link-1 and Link-2 (dotted line, right *y*-axis). (b) Fusion kinetics shown as extent of mixing over time, with [thrombin] = 200 nM. Error bars represent 95% CI.

over a range of 0−1600 nM thrombin (52% at 1600 nM thrombin).

Experimentally, emulsions were prepared with concentrations of 1.3 mM DPPC, 40 μM DSPE-PEG2000, and 0.65 μM Chol-DNA; more DSPE-PEG2000 was added than with previous studies to reduce the nonspecific binding of the thrombin to the lipid monolayer. The concentration of droplets in this preparation was also increased to 2×10^{12} mL^{-1} to enhance fusion. Additionally, the DNA concentration was adjusted to obtain a final concentration of all DNA strands to be ∼135 nM in the final mixtures. During vesicle preparation, an excess amount of TA (1.0 μM) was added to hybridize to the free end of Link-1 strands. For the thrombin experiments, the droplets containing Link-1 and TA strands were mixed with Link-2 droplets in the presence of thrombin ranging from 0 to 800 nM at 37 °C for 45 min. The droplets were then imaged and processed as before, and the extent of mixing was plotted against thrombin concentration (Figure 5a). For the droplets without thrombin, the extent of mixing was the same as that of droplets without DNA (below 5%) at the time of mixing, although after 45 min mixing increased to 13%, most likely due to partial removal of the strand through competition with Link-2. With increasing thrombin concentration up to 400 nM, the extent of mixing increased similarly to the fitted curve. The extent of mixing decreased at 800 nM, most likely due to prevention of fusion through nonspecific binding of the thrombin to the lipid monolayer. Without the TA blocking strand, the fusion increased to 41% after 45 min. The increase in droplet fusion up to 400 nM appeared to match the predicted model. At higher concentrations, we hypothesize that the thrombin begins to adhere to the emulsion surface, inhibiting fusion. Fusion kinetics in the presence of thrombin was also evaluated and shown here for a thrombin concentration of 200 nM (Figure 5b). The percent mixing increased to saturation levels within 15 min of incubating the droplets with thrombin. The thrombin aptamer blocks the fusion process initially. With the addition of thrombin, TA

dx.doi.org/10.1021/la502483u | *Langmuir* 2014, 30, 12321−12327

strand is removed and droplet fusion occurs within a period of 15 min.

As a counterexample to fusion-driven detection, a system in which different thrombin aptamers were anchored to droplet surfaces was evaluated for its ability to promote content mixing. Two different thrombin aptamer sequences were incorporated into the lipid interface of droplets: 5′Chol-TEG/TTT TTG GTT GGT GTG GTT GG/3′ (TA1),[49] which binds to the fibrinogen-binding site of thrombin, and 5′/AGT CCG TGG TAG GGC AGG TTG GGG TGA CCT TTT T/3′Chol-TEG (TA2),[51] which binds to the heparin-binding site of thrombin. Two sets of droplets containing either aptamer TA1 or TA2 were loaded with BPEA and DiI in their internal phases (5CB), respectively. Confocal images were taken after 45 min incubation with different concentrations of thrombin to monitor fusion of droplets. Colocalization analysis was conducted as discussed in previous sections, and the fusion efficacy of thrombin aptamer loaded droplets in the presence of thrombin was determined. Without thrombin, the droplets did not aggregate (Figure 6a), but with addition of 1000 nM thrombin they formed aggregates (Figure 6b). Despite thrombin driving aggregation, however, overall content mixing was low (Figure 6c), and hence, this form of sandwich-type binding was not optimal for designing signal-generating assays using content mixing of droplets.

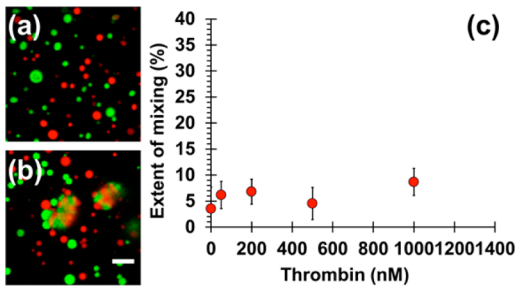

Figure 6. 5CB droplets with thrombin aptamers (TA1 and TA2) incubated with varying concentrations of thrombin: Merged fluorescent images of BPEA (green) and DiI (red) in 5CB droplets (a) without thrombin and (b) with 1000 nM thrombin. (c) Extent of mixing of droplets as a function of thrombin concentration.

4. CONCLUSION

In conclusion, a new method was developed for the directed fusion of droplets in bulk without flow focusing or microfluidics. Inspired by SNARE complexes in cells, the fusion process was mediated by the interaction of DNA strands in a "head-to-head" orientation, and the extent of content mixing was determined through analysis of confocal microscopy images. Using a combination of fluid-phase lipid monolayers to allow lipid mixing and PEG-lipid conjugates to prevent nonspecific binding, emulsions containing complementary DNA strands were found to fuse at about 40%, compared with a nonspecific background of about 3-5%. In addition, by utilizing the competitive binding of an aptamer and thrombin, the emulsions could also be used as an in-solution sensor for protein targets without additional washing steps required in most of the commercial ELISA assays. Future efforts will involve increasing the sensitivity of the assay and designing novel detection platforms by combining the content-mixing capabilities of these droplets with other sensing modalities such as chemiluminescence, ultrasound detection, or magneto-resistance. In future work, the surface structure of the emulsions will be optimized further to allow sensing in more complex biological media to create rapid, in-solution sensors.

■ ASSOCIATED CONTENT

Supporting Information

Data showing calculations for nearest neighbor model, fluorescence studies of DNA incorporation into monolayer, histogram of fractional mixing of droplets, and the effect of fusion on average diameter. This material is available free of charge via the Internet at http://pubs.acs.org.

■ AUTHOR INFORMATION

Corresponding Author

*E-mail: andrew.goodwin@colorado.edu.

Author Contributions

The manuscript was written through contributions of all authors. All authors have given approval to the final version of the manuscript.

Notes

The authors declare no competing financial interest.

■ ACKNOWLEDGMENTS

The authors thank Dr. Theodore Randolph for use of his dynamic light scattering instrument and his lab members for help with measurements, as well as Dr. Kevin Dean for help with confocal microscopy. The authors also thank Prof. Daniel Schwartz for helpful discussions. A. P. G. thanks the National Institutes of Health for a Pathway to Independence Award in Cancer Nanotechnology (R00-CA153935), which funded this research. P.S.N. thanks the National Science Foundation (Award CBET-1160202) and the Liquid Crystal Materials Research Center (NSF/MRSEC, Award DMR-820579) for financial support. NIH R00-CA153935; NSF CBET-1160202, NSF/MRSEC DMR-820579.

■ REFERENCES

(1) Chen, H.; Li, J.; Shum, H. C.; Stone, H. A.; Weitz, D. A. Breakup of double emulsions in constrictions. *Soft Matter* **2011**, *7*, 2345−2347.
(2) Link, D. R.; Anna, S. L.; Weitz, D. A.; Stone, H. A. Geometrically mediated breakup of drops in microfluidic devices. *Phys. Rev. Lett.* **2004**, *92*, 054503.
(3) Utada, A. S.; Fernandez-Nieves, A.; Stone, H. A.; Weitz, D. A. Dripping to jetting transitions in coflowing liquid streams. *Phys. Rev. Lett.* **2007**, *99*, 094502.
(4) Utada, A. S.; Lorenceau, E.; Link, D. R.; Kaplan, P. D.; Stone, H. A.; Weitz, D. A. Monodisperse double emulsions generated from a microcapillary device. *Science* **2005**, *308*, 537−41.
(5) Südhof, T. C.; Rothman, J. E. Membrane Fusion: Grappling with SNARE and SM proteins. *Science* **2009**, *323*, 474−477.
(6) Sutton, R. B.; Fasshauer, D.; Jahn, R.; Brunger, A. T. Crystal structure of a SNARE complex involved in synaptic exocytosis at 2.4 A resolution. *Nature* **1998**, *395*, 347−353.
(7) Robson Marsden, H.; Elbers, N. A.; Bomans, P. H.; Sommerdijk, N. A.; Kros, A. A reduced SNARE model for membrane fusion. *Angew. Chem., Int. Ed. Engl.* **2009**, *48*, 2330−2333.
(8) Gong, Y.; Luo, Y. M.; Bong, D. Membrane activation: Selective vesicle fusion via small molecule recognition. *J. Am. Chem. Soc.* **2006**, *128*, 14430−14431.
(9) Chan, Y. H. M.; van Lengerich, B.; Boxer, S. G. Lipid-anchored DNA mediates vesicle fusion as observed by lipid and content mixing. *Biointerphases* **2008**, *3*, Fa17−Fa21.
(10) Stengel, G.; Simonsson, L.; Campbell, R. A.; Hook, F. Determinants for membrane fusion induced by cholesterol-modified DNA zippers. *J. Phys. Chem. B* **2008**, *112*, 8264−8274.

(11) Simonsson, L.; Jonsson, P.; Stengel, G.; Höök, F. Site-specific DNA-controlled fusion of single lipid vesicles to supported lipid bilayers. *ChemPhysChem* **2010**, *11*, 1011−1017.
(12) Stengel, G.; Simonsson, L.; Campbell, R. A.; Höök, F. Determinants for membrane fusion induced by cholesterol-modified DNA zippers. *J. Phys. Chem. B* **2008**, *112*, 8264−8274.
(13) Stengel, G.; Zahn, R.; Höök, F. DNA-induced programmable fusion of phospholipid vesicles. *J. Am. Chem. Soc.* **2007**, *129*, 9584−9585.
(14) Nakatsuka, M. A.; Barback, C. V.; Fitch, K. R.; Farwell, A. R.; Esener, S. C.; Mattrey, R. F.; Cha, J. N.; Goodwin, A. P. In vivo ultrasound visualization of non-occlusive blood clots with thrombin-sensitive contrast agents. *Biomaterials* **2013**, *34*, 9559−65.
(15) Nakatsuka, M. A.; Hsu, M. J.; Esener, S. C.; Cha, J. N.; Goodwin, A. P. DNA-coated microbubbles with biochemically tunable ultrasound contrast activity. *Adv. Mater.* **2011**, *23*, 4908−4912.
(16) Nakatsuka, M. A.; Lee, J. H.; Nakayama, E.; Hung, A. M.; Hsu, M. J.; Mattrey, R. F.; Esener, S. C.; Cha, J. N.; Goodwin, A. P. Facile one-pot synthesis of polymer-phospholipid composite microbubbles with enhanced drug loading capacity for ultrasound-triggered therapy. *Soft Matter* **2011**, *2011*, 1656−1659.
(17) Nakatsuka, M. A.; Mattrey, R. F.; Esener, S. C.; Cha, J. N.; Goodwin, A. P. Aptamer-crosslinked microbubbles: smart contrast agents for thrombin-activated ultrasound imaging. *Adv. Mater.* **2012**, *24*, 6010−6016.
(18) Chomas, J. E.; Dayton, P.; May, D.; Ferrara, K. Threshold of fragmentation for ultrasonic contrast agents. *J. Biomed. Opt.* **2001**, *6*, 141−150.
(19) Ferrara, K.; Pollard, R.; Borden, M. Ultrasound microbubble contrast agents: Fundamentals and application to gene and drug delivery. *Annu. Rev. Biomed. Eng.* **2007**, *9*, 415−447.
(20) Ferrara, K. W. Driving delivery vehicles with ultrasound. *Adv. Drug. Delivery Rev.* **2008**, *60*, 1097−1102.
(21) Borden, M. A.; Kruse, D. E.; Caskey, C. F.; Zhao, S.; Dayton, P. A.; Ferrara, K. W. Influence of lipid shell physicochemical properties on ultrasound-induced microbubble destruction. *IEEE Trans. Ultrason. Ferroelectr. Freq. Control* **2005**, *52*, 1992−2002.
(22) Klibanov, A. L. Targeted delivery of gas-filled microspheres, contrast agents for ultrasound imaging. *Adv. Drug. Delivery Rev.* **1999**, *37*, 139−157.
(23) Noonan, P. S.; Mohan, P.; Goodwin, A. P.; Schwartz, D. K. DNA hybridization-mediated liposome fusion at the aqueous liquid crystal interface. *Adv. Funct. Mater.* **2014**, *24*, 3206−3212.
(24) Schneider, C. A.; Rasband, W. S.; Eliceiri, K. W. NIH Image to ImageJ: 25 years of image analysis. *Nat. Methods* **2012**, *9*, 671−675.
(25) Elghanian, R.; Storhoff, J. J.; Mucic, R. C.; Letsinger, R. L.; Mirkin, C. A. Selective colorimetric detection of polynucleotides based on the distance-dependent optical properties of gold nanoparticles. *Science* **1997**, *277*, 1078−81.
(26) Mirkin, C. A.; Letsinger, R. L.; Mucic, R. C.; Storhoff, J. J. A DNA-based method for rationally assembling nanoparticles into macroscopic materials. *Nature* **1996**, *382*, 607−609.
(27) Hung, A. M.; Micheel, C. M.; Bozano, L. D.; Osterbur, L. W.; Wallraff, G. M.; Cha, J. N. Large-area spatially ordered arrays of gold nanoparticles directed by lithographically confined DNA origami. *Nat. Nanotechnol.* **2010**, *5*, 121−126.
(28) Kershner, R. J.; Bozano, L. D.; Micheel, C. M.; Hung, A. M.; Fornof, A. R.; Cha, J. N.; Rettner, C. T.; Bersani, M.; Frommer, J.; Rothemund, P. W.; Wallraff, G. M. Placement and orientation of individual DNA shapes on lithographically patterned surfaces. *Nat. Nanotechnol.* **2009**, *4*, 557−561.
(29) Lee, J. B.; Roh, Y. H.; Um, S. H.; Funabashi, H.; Cheng, W.; Cha, J. J.; Kiatwuthinon, P.; Muller, D. A.; Luo, D. Multifunctional nanoarchitectures from DNA-based ABC monomers. *Nat. Nanotechnol.* **2009**, *4*, 430−436.
(30) Hadorn, M.; Boenzli, E.; Sorensen, K. T.; Fellermann, H.; Eggenberger Hotz, P.; Hanczyc, M. M. Specific and reversible DNA-directed self-assembly of oil-in-water emulsion droplets. *Proc. Natl. Acad. Sci. U. S. A.* **2012**, *109*, 20320−20325.
(31) Garg, S.; Thomas, A. A.; Borden, M. A. The effect of lipid monolayer in-plane rigidity on in vivo microbubble circulation persistence. *Biomaterials* **2013**, *34*, 6862−6870.
(32) Lichtenberg, D.; Menashe, M.; Donaldson, S.; Biltonen, R. L. Thermodynamic characterization of the pretransition of unilamellar dipalmitoyl-phosphatidylcholine vesicles. *Lipids* **1984**, *19*, 395−400.
(33) van Lengerich, B.; Rawle, R. J.; Bendix, P. M.; Boxer, S. G. Individual vesicle fusion events mediated by lipid-anchored DNA. *Biophys. J.* **2013**, *105*, 409−419.
(34) Agirre, A.; Nir, S.; Nieva, J. L.; Dijkstra, J. Induction of aggregation and fusion of cholesterol-containing membrane vesicles by an anti-cholesterol monoclonal antibody. *J. Lipid. Res.* **2000**, *41*, 621−628.
(35) Tuerk, C.; Gold, L. Systematic evolution of ligands by exponential enrichment: RNA ligands to bacteriophage T4 DNA polymerase. *Science* **1990**, *249*, 505−10.
(36) Ellington, A. D.; Szostak, J. W. In vitro selection of RNA molecules that bind specific ligands. *Nature* **1990**, *346*, 818−822.
(37) Nutiu, R.; Li, Y. Structure-switching signaling aptamers. *J. Am. Chem. Soc.* **2003**, *125*, 4771−4778.
(38) Xiang, Y.; Xie, M.; Bash, R.; Chen, J. J.; Wang, J. Ultrasensitive label-free aptamer-based electronic detection. *Angew. Chem.* **2007**, *46*, 9054−9056.
(39) Huang, C. C.; Huang, Y. F.; Cao, Z.; Tan, W.; Chang, H. T. Aptamer-modified gold nanoparticles for colorimetric determination of platelet-derived growth factors and their receptors. *Anal. Chem.* **2005**, *77*, 5735−5741.
(40) Li, W.; Wang, K.; Tan, W.; Ma, C.; Yang, X. Aptamer-based analysis of angiogenin by fluorescence anisotropy. *Analyst* **2007**, *132*, 107−113.
(41) Liu, G.; Mao, X.; Phillips, J. A.; Xu, H.; Tan, W.; Zeng, L. Aptamer-nanoparticle strip biosensor for sensitive detection of cancer cells. *Anal. Chem.* **2009**, *81*, 10013−10018.
(42) Pu, Y.; Liu, H.; Liu, B.; Liao, J.; Liu, J.; Zhao, Z.; Tan, W. Development of aptamer-based nanomaterials for biological analysis. *Curr. Mol. Med.* **2013**, *13*, 681−689.
(43) Xu, Y.; Phillips, J. A.; Yan, J.; Li, Q.; Fan, Z. H.; Tan, W. Aptamer-based microfluidic device for enrichment, sorting, and detection of multiple cancer cells. *Anal. Chem.* **2009**, *81*, 7436−7442.
(44) Zhang, J.; Liu, B.; Liu, H.; Zhang, X.; Tan, W. Aptamer-conjugated gold nanoparticles for bioanalysis. *Nanomedicine* **2013**, *8*, 983−993.
(45) Zhu, G.; Zheng, J.; Song, E.; Donovan, M.; Zhang, K.; Liu, C.; Tan, W. Self-assembled, aptamer-tethered DNA nanotrains for targeted transport of molecular drugs in cancer theranostics. *Proc. Natl. Acad. Sci. U. S. A.* **2013**, *110*, 7998−8003.
(46) Jiang, Z.; Yang, T.; Liu, M.; Hu, Y.; Wang, J. An aptamer-based biosensor for sensitive thrombin detection with phthalocyanine@SiO_2 mesoporous nanoparticles. *Biosens. Bioelecton.* **2014**, *53*, 340−345.
(47) Wang, J.; Zhu, G.; You, M.; Song, E.; Shukoor, M. I.; Zhang, K.; Altman, M. B.; Chen, Y.; Zhu, Z.; Huang, C. Z.; Tan, W. Assembly of aptamer switch probes and photosensitizer on gold nanorods for targeted photothermal and photodynamic cancer therapy. *ACS Nano* **2012**, *6*, 5070−5077.
(48) Yuan, Q.; Wu, Y.; Wang, J.; Lu, D.; Zhao, Z.; Liu, T.; Zhang, X.; Tan, W. Targeted bioimaging and photodynamic therapy nanoplatform using an aptamer-guided G-quadruplex DNA carrier and near-infrared light. *Angew. Chem.* **2013**, *52*, 13965−13969.
(49) Bock, L. C.; Griffin, L. C.; Latham, J. A.; Vermaas, E. H.; Toole, J. J. Selection of single-stranded DNA molecules that bind and inhibit human thrombin. *Nature* **1992**, *355*, 564−566.
(50) SantaLucia, J. A unified view of polymer, dumbbell, and oligonucleotide DNA nearest-neighbor thermodynamics. *Proc. Natl. Acad. Sci. U. S. A.* **1998**, *95*, 1460−1465.
(51) Tasset, D. M.; Kubik, M. F.; Steiner, W. Oligonucleotide inhibitors of human thrombin that bind distinct epitopes. *J. Mol. Biol.* **1997**, *272*, 688−698.